

Modeling of post-tensioned one-way and two-way slabs with unbonded tendons

Uksun Kim^{1a}, Yu Huang^{2b}, Pinaki R. Chakrabarti^{1c} and Thomas H.-K. Kang^{*3}

¹Department of Civil Engineering, California State University at Fullerton,
800 N. State College Blvd., Fullerton, CA 92834, U.S.A.

²School of Civil Engineering and Environmental Science, The University of Oklahoma,
202 W. Boyd St. Rm 334, Norman, OK 73019, U.S.A.

³Department of Architecture & Architectural Engineering, Seoul National University,
1 Gwanak-ro, Gwanak-gu, Seoul 151-744, Republic of Korea

(Received July 29, 2013, Revised February 4, 2014, Accepted May 22, 2014)

Abstract. A sophisticated finite element modeling approach is proposed to simulate unbonded post-tensioned concrete slabs. Particularly, finite element contact formulation was employed to simulate the sliding behavior of unbonded tendons. The contact formulation along with other discretizing schemes was selected to assemble the post-tensioned concrete system. Three previously tested unbonded post-tensioned two-way and one-way slabs with different reinforcement configurations and boundary conditions were modeled. Numerical results were compared against experimental data in terms of global pressure-deflection relationship, stiffness degradation, cracking pattern, and stress variation in unbonded tendons. All comparisons indicate a very good agreement between the simulations and experiments. The exercise of model validation showcased the robustness and reliability of the proposed modeling approach applied to numerical simulation of post-tensioned concrete slabs.

Keywords: post-tensioning; prestressed concrete; two-way slabs; finite element; numerical model

1. Introduction

Since the first post-tensioning method applied in U.S. buildings in the mid to late 1950s (PTI 2006; Klemencic *et al.* 2006; Chacos 2007; Bondy 2012), unbonded post-tensioned (PT) slabs are widely used in the buildings, especially for parking structures. Recently, PT slab systems are used not only for parking structures but also high-rise office buildings to reduce story heights. Regardless of widespread use of PT slabs in building construction, nonlinear structural behavior of unbonded one-way and two-way PT slabs are not fully deciphered. Using a reliable finite element model, this topic can be investigated effectively instead of expensive and labor-intensive experimental studies. According to this demand, a 3-D finite element model of unbonded PT slabs

*Corresponding author, Associate Professor, E-mail: tkang@snu.ac.kr

^aAssociate Professor

^bPh.D.

^cProfessor

has been developed in this study.

Until now, there are not many research papers for numerical modeling of unbonded PT members. Kim *et al.* (2009) developed a sophisticated 3-D finite element model for simulating the nonlinear flexural behavior of unbonded PT beams. To verify the accuracy of the proposed 3-D finite element model, numerical analysis results were compared with experimental results. Furthermore, very limited research work has been performed for numerical modeling of unbonded PT slabs. The finite element procedure proposed by Van Greunen and Scordelis (1983) was able to analyze both of bonded and unbonded pre-stressed slabs. The procedure was incorporated into a computer program, which is capable of analyzing the prestressed slabs with the consideration of time dependent effects, material and geometric nonlinearities. Two numerical analyses were carried out in the study including a pre-tensioned concrete column tested by Aroni (1968) and a continuous two-way unbonded PT slab tested by Scordelis *et al.* (1959). The analysis maintained a good agreement with the experiment for the pre-tensioned column, while the modeling scheme was partially consistent with the PT slab test data in the inelastic range. Van Greunen and Scordelis (1983) explained that the discrepancies found at the failure stage were caused by the coarse mesh and difficulty of modeling the actual tendon forces at major interior cracks. Recently, Rabczuk and Zi (2008), Kwak and Son (2010), and Vecchio *et al.* (2006) modeled the unbonded or bonded tendon behavior in conjunction with concrete structures.

The objectives of this research are: 1) to propose reliable numerical models which can trace the nonlinear behavior of unbonded PT one-way and two-way slabs with accuracy; 2) to compare the overall structural behaviors of unbonded PT slabs through testing and simulation; 3) to investigate crack propagation, strain, pressure, and deflection of unbonded PT slabs through testing and simulation. This paper is a journal version paper which has been developed based on the short version conference paper (Kim *et al.* 2011) of the 2011 International Conference on Computational Technologies in Concrete Structures and the Conference Chair's recommendation.

2. Structural tests of post-tensioned slabs

2.1 Test specimens

Three two-way PT slabs (PTS-1, PTS-2 and PTS-6) and three one-way PT slabs (PTS-3, PTS-4 and PTS-5) were tested as listed in Table 1. All slabs were reinforced with unbonded post-tensioning tendons and bonded mild steel. Table 2 summarizes the dimensions and boundary conditions of each specimen. The two-way slabs (PTS-1, PTS-2, and PTS-6) were simply supported on four sides of the slab with some rotation allowed. The one-way slab specimens had three different boundary conditions on span ends: 1) PTS-3 had fixed conditions on both ends; 2) PTS-4 was pinned on one end and fixed on the other end; and 3) PTS-5 was pinned conditions on both ends.

Slab thickness was 76 mm for all specimens. PTS-1, PTS-2, and PTS-6 (two-way slab) had a footprint of 2.76 m by 2.76 m including end supports, and the clear span length in each principal direction was 2.7 m (Fig. 1). Mild steel wire mesh with a size of 2.13 m by 2.13 m was placed at the compression surface of each slab mainly to prevent damage during transportation. The amount of mild steel, which varied for each specimen, is provided in Table 1. The simple support fully restrained the slab vertical displacement at the edge with a clamp.

The one-way slabs (PTS-3, PTS-4 and PTS-5) had various footprints depending on the support

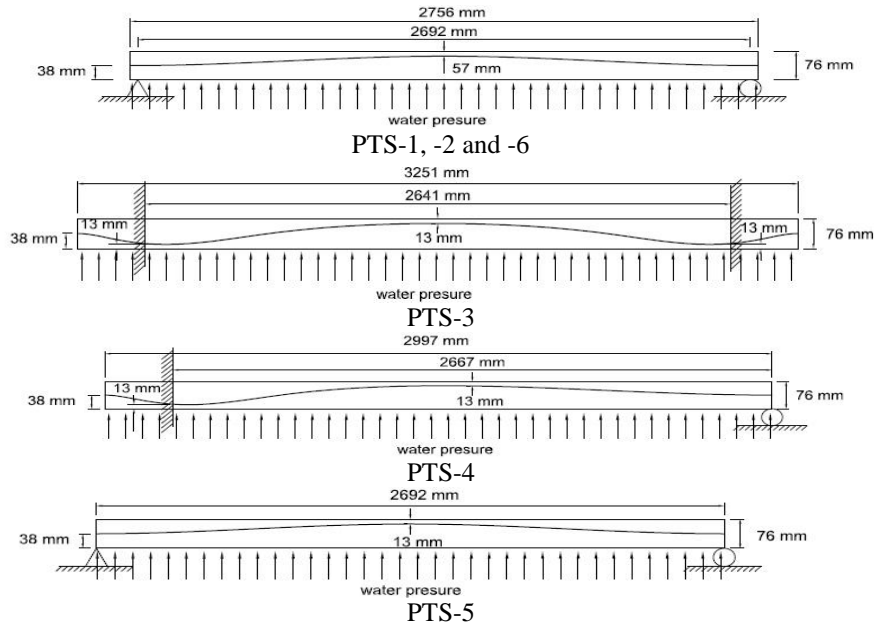


Fig. 1 Draped tendon profiles and loading conditions for test specimens

Table 1 Summary of steel reinforcement and measured concrete strength for specimens

Specimens	Post-tensioning tendons per unit width (A_{ps}), mm^2/mm	Tensile mild steel per unit width (A_{ps}), mm^2/mm	Compressive mild steel per unit width (A_{ps}), mm^2/mm	f'_c , MPa
PTS-1 (two-way)	16-6.35 mm strands ea. way (0.14)	4 x 4-4/4 WWM 102x102 MW 25.8/25.8 (0.254)	6 x 6-10/10 WWM 152x152 MW 9.1/9.1 (0.06)	40.9
PTS-2 (two-way)	16-6.35 mm strands ea. way (0.14)	6 x 6-10/10 WWM 152x152 MW 9.1/9.1 (0.06)	6 x 6-10/10 WWM 152x152 MW 9.1/9.1 (0.06)	41.1
PTS-3 (one-way)	16-6.35 mm strands in span direction (0.14)	25-9.5 mm at top & 9-No. 3 at bottom ea. fixed end (0.673)	6 x 6-10/10 WWM 152x152 MW 9.1/9.1 (0.06)	39.5
PTS-4 (one-way)	16-6.35 mm strands in span direction (0.14)	26-9.5 mm at top & 9-9.5 mm at bottom ea. fixed end (0.7)	6 x 6-10/10 WWM 152x152 MW 9.1/9.1 (0.06)	41.1
PTS-5 (one-way)	16-6.35 mm strands in span direction (0.14)	27-9.5 mm at top & 9-9.5 mm at bottom ea. fixed end (0.673)	6 x 6-10/10 WWM 152x152 MW 9.1/9.1 (0.06)	37
PTS-6 (two-way)	16-6.35 mm strands ea. way (0.14)	6 x 6-10/10 WWM 152x152 MW 9.1/9.1 (0.06)	6 x 6-10/10 WWM 152x152 MW 9.1/9.1 (0.06)	36

 WWM = Welded Wire Mesh; f'_c = Concrete compressive strength

Table 2 Dimensions for test specimens

Specimens	l_1	l_{c1}	l_2	l_{c2}	Boundary Condition
PTS-1, PTS-2 and PTS-6	2,756 mm	2,692 mm	2,756 mm	2,692 mm	Pin-Pin
PTS-3	3,251 mm	2,642 mm	2,642 mm	2,642 mm	Fixed-Fixed
PTS-4	2,997 mm	2,667 mm	2,642 mm	2,642 mm	Fixed-Pin
PTS-5	2,692 mm	2,692 mm	2,642 mm	2,642 mm	Pin-Pin

l_1 = Slab length in the span or one direction;

l_{c1} = Support center-to-support center length in the span or one direction;

l_2 = Slab length in the transverse or the other direction;

l_{c2} = Support center-to-support center length in the transverse or the other direction.

boundary conditions as indicated in Table 2 and Fig. 1. Twenty-five No. 3 ($d_b = 9.5$ mm) tension bars were placed at a spacing of 102 mm in the span direction of the one-way slabs, and nine No.3 bars were placed as tension reinforcement at a spacing of 356 mm at the fixed end of the one-way slabs. Additionally, the 6 x 6 – 10/10 (152 x 152 MW 9.1/9.1) wire meshes were used for all one-way slab specimens to prevent cracks during installation of the specimens.

Fig. 1 shows the draped tendon profiles and loading conditions used for the specimens. The pressure was applied upward through the hydraulic water bag which was located under the PT slab specimens, so the top surface of the slabs at mid-span was referred to as the tension side. Fig. 2 shows the post-tensioning reinforcement layout plan for the specimens. A total of sixteen post-tensioning tendons were placed in each direction of the two-way slabs, and in the span direction of the one-way slabs. The spacing of uniformly distributed tendons was 152 mm for the two-way slabs, and thus the cross-sectional area of the tendons per unit width was $0.15 \text{ mm}^2/\text{mm}$. For the one-way slab, two tendons were grouped with a spacing of 57 mm between each tendon, and the two-tendon group was then uniformly distributed with a spacing of 305 mm between the groups. Post-tensioning tendons were stressed to about $0.7f_{pu}$ before transfer, resulting in an effective stress (f_{se}) of about $0.65f_{pu}$ after transfer, where f_{pu} is the specified tensile strength of prestressing steel. More detailed information regarding the specimens is available elsewhere (Kim *et al.* 2012).

2.2 Materials

Normal-weight concrete with a design compressive strength of 34.5 MPa was used. Concrete mixes were prepared according to ASTM C-94-05 (ASTM 2008). The concrete was proportioned using Portland cement and fly ash with a water-cementitious materials ratio of 0.34 (weight per volume ratio), resulting in a slump of about 76 mm. The concrete compressive strength measured at test date for each specimen is indicated in Table 1. The average measured concrete strength was 39.2 MPa.

For post-tensioning, 6.35 mm diameter 7-wire strands were used in each direction of the two-way slabs and in the span direction of one-way slabs. These were Grade 270 ASTM A-416 strands (ASTM 2008) with a specified ultimate strength (f_{pu}) of 1862 MPa and cross-sectional area (A_{ps}) of 23.2 mm^2 . The individual prestressing strands were inserted through 7.1 mm inner diameter plastic tubes.

Two different types of non-prestressed mild steel were used: 1) Welded Wire Mesh (WWM) produced in accordance with ASTM A-185 and 2) ASTM A-615 deformed reinforcing bars

(ASTM 2008). For the tension mild steel of two-way slabs, the WWM with a specified yield strength of 414 MPa was used, whereas Grade 60 No. 3 ($d_b = 9.5$ mm) reinforcing bars with a specified yield strength of 414 MPa were used as tension reinforcement of the one-way slabs (Table 1).

2.3 Test setup and procedure

All of six post-tensioned slabs were tested under uniformly distributed area loads or pressure by using a hydraulic water bag (Figs. 1 and 3). The water pressure was gradually increased at approximately 6.9 kPa increments.

Testing was stopped when the slabs reached anyone of the following three criteria: 1) when excessive cracks (several large cracks at the edges) were visually observed; 2) when the deflection in the slab reached close to $L/120$, where L is the span length; and 3) when the post-tensioning stress reached nearly 75% to 85% of the ultimate tensile strength ($0.75f_{pu}$ to $0.85f_{pu}$).

During the testing, a wide variety of measurements were monitored (Fig. 3), including pressure, deflection, strain (in mild steel), and change in post-tensioning forces. The applied pressure was monitored by the pressure gauge. The displacement transducers used to measure the deflection were linear variable differential transformers (LVDTs) with 100 mm of travel. Strain gauges were mounted on the steel rebar or wire mesh at mid-span and end support. Load cells were placed at the ends of the unbonded post-tensioning tendons to record the post-tensioning forces during the post-tensioning and external loading.



Fig. 2 Tendon layout for one-way and two-way slabs



Fig. 3 Test set-up for one-way slabs (PTS-4) under uniformly distributed pressure (Bottom: fixed support end; top: pin support end)

3. Numerical modelling & analysis of post tensioned slabs

In this section, the modeling details of one-way and two-way post-tensioned slabs using ABAQUS, advanced finite element analysis software (HKS 2011), are described which includes material assumptions, element types and analysis procedures

3.1 Concrete modeling

Concrete is simulated by a built-in “Concrete Damaged Plasticity” constitutive relation in ABAQUS. The damage factors that define stiffness degradation are neglected in the simulation primarily due to the monotonic loading used in the experiment. It has been confirmed that the behavior of post-tensioned concrete members under monotonic loads is not sensitive to damage factors, especially when the compressive damage is not dominant (Huang *et al.* 2010). The uniaxial stress-strain relation in compression is defined according to the model proposed by Carreira and Chu (1985). The tensile behavior is assumed to be linear before reaching tensile strength, defined as $f_{cr} = 0.625\sqrt{f'_c}$. A so-called tension stiffening effect is used to simplify interactions of concrete and deformed bars when cracking occurs. For heavily reinforced members, tension stiffening is suggested such that the stress reduces to zero at a total strain of about ten times the strain at cracking (HKS 2011). Such large tension stiffening could introduce unreasonable mesh sensitivity for lightly reinforced members like PT slabs. Therefore, when the stress reduces to a residual (non-zero) stress, the strain is set to be about two times the strain at cracking in this study. Other factors were defined so as to yield the best results of analyses of slabs with and without prestressed reinforcement (Huang *et al.* 2011). For example, the dilation angle was set as 50° .

3.2 Steel modeling

An elasto-perfectly plastic model is employed for modeling conventional non-prestressed mild steel. The bilinear uniaxial stress-strain relationship along with a yield stress of f_y and elastic modulus of E_s is reasonably accurate to define the mild steel behavior, because all simulations are monotonically loaded. Conversely, prestressing steel is modeled by using an empirical nonlinear stress-strain model developed by Devalapura and Tadros (1992) for Grade 270 seven-wire strands. This nonlinear stress-strain relation is simplified to be piecewise linear. All uniaxial nominal stress-strain relations used in this study are converted into true stress-strain relations for material data input.

3.3 Elements

Non-prestressed mild steel and prestressing steel are modeled using three dimensional 2-node linear truss elements (T3D2 in ABAQUS element library). Concrete and tendon sheathing are formulated by using three dimensional 8-node linear brick elements with the reduced integration rule (C3D8R in ABAQUS element library). Five layers are arranged in the vertical direction of slabs, ensuring the accuracy of bending stiffness. Typical dimension of an element is about 25.4 mm for all models. Fig. 4 shows the mesh generation for PTS-1 using ABAQUS.

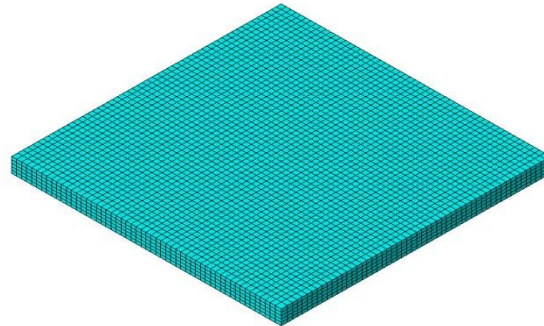


Fig. 4 Mesh arrangement for PTS-1

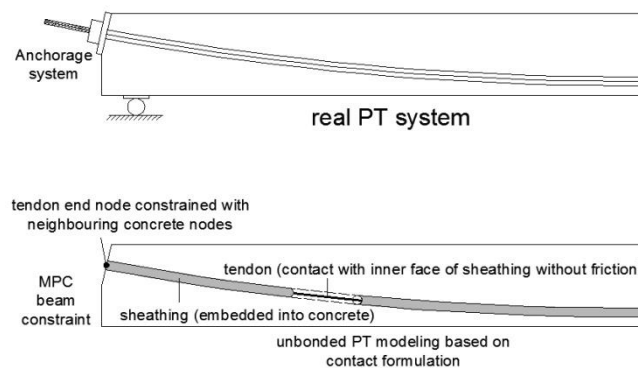


Fig. 5 Modeling of unbonded PT systems

3.4 Interactions between steel and concrete elements

Non-prestressed mild steel is assumed to be perfectly bonded, which can be achieved by using the “Embedded region” constraint. Nodes of mild steel elements embedded into concrete elements are displacement compatible with concrete nodes, which ensures perfect bonding. The sheathing elements are also embedded into concrete elements to ensure compatibility of deformation. The unbonded condition between prestressing steel and sheathing is directly simulated using “surface-to-surface contact” in ABAQUS/Explicit formulation. The penalty method is employed to enforce the contact constraint. The selected contact formulation physically models the behavior of the prestressing steel and sheathing that are in contact with each other. The tangential behavior of the contact is frictionless which allows the tendon to be free of slip. The assumption of idealized frictionless contact for unbonded tendons is reasonable (Vecchio *et al.* 2006, Kang and Wallace 2008). The Beam Multiple-Points Constraints (MPC) is used, providing a rigid beam between nodes of an unbonded tendon and an anchorage, such that the deformation compatibility at the anchorage location is achieved. An overview of modeling of unbonded tendon systems is illustrated in Fig. 5. Figs. 6 and 7 show the meshed slab models with unbonded tendons for one-way and two-way slabs.

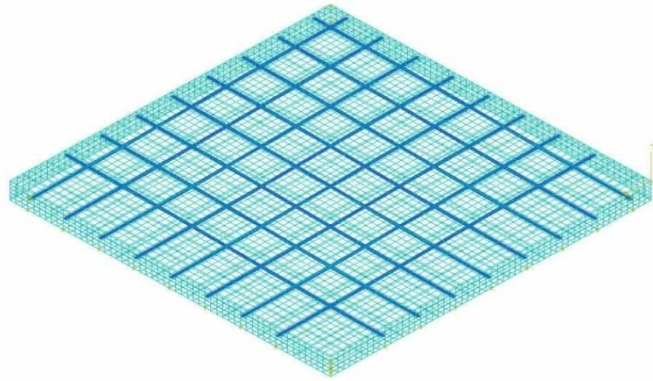


Fig. 6 Modeling of two-way PT slab systems (PTS-1)

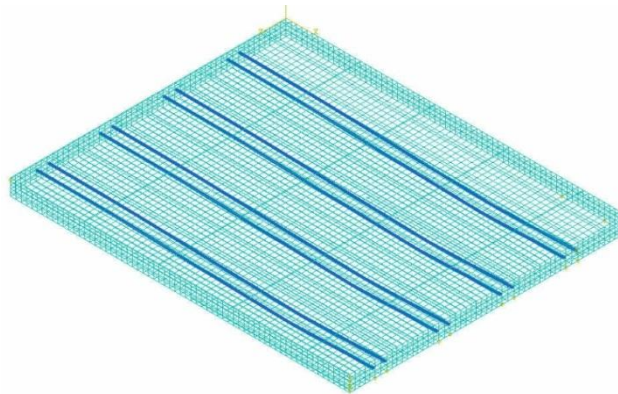


Fig. 7 Modeling of one-way PT slab systems (PTS-3)

3.5 Analysis procedures

Two analysis steps are included in the simulations to represent prestressing and external loading stages, respectively. The frictionless nature of unbonded tendons is maintained from the initial step of the simulations. The explicit dynamic analysis is employed for all simulations to guarantee converged solutions. The small tension stiffening effect introduced for concrete material causes great material nonlinearity due to violent cracking. Consequently, conventional nonlinear numerical scheme frequently suffers and fails to reach a solution. The tested slabs were subjected to uniformly distributed pressure, which was applied vertically upward. All simulations carried out in this study are force-controlled.

4. Numerical modelling & analysis of post tensioned slabs

In this study, total six PT slabs (one-way & two-way) were tested and among them, three (PTS-1, PTS-3 and PTS-5) were chosen based on the reliability of the test data and boundary conditions. These three PT slabs were modeled, simulated and compared with test results.

4.1 Cracking

Fig. 8 shows the crack patterns (analysis vs. test) on the tension surface and Fig. 9 shows cracks in one direction (analysis vs. test). The crack patterns generated from numerical analysis can be well matched with the crack patterns observed from the tests as shown in Figs. 8 and 9. The compression (bottom) surface of each specimen was not accessible for observation of cracks during testing. After the first crack appeared in the tension (top) surface, additional cracks were marked and crack patterns were recorded. As expected, diagonal cracking patterns were observed in the two-way slab (PTS-1). Since the square panel with the same reinforcing details in two principal directions was tested, the crack patterns were symmetrical with respect to both principal axes (Fig. 8). The symmetric cracks observed from the two-way slabs indicate that the area load/pressure was quite uniformly applied on the slabs. For the one-way slabs (PTS-3 and PTS-5), flexural cracks were concentrated on the tension (top) surface at the location where positive

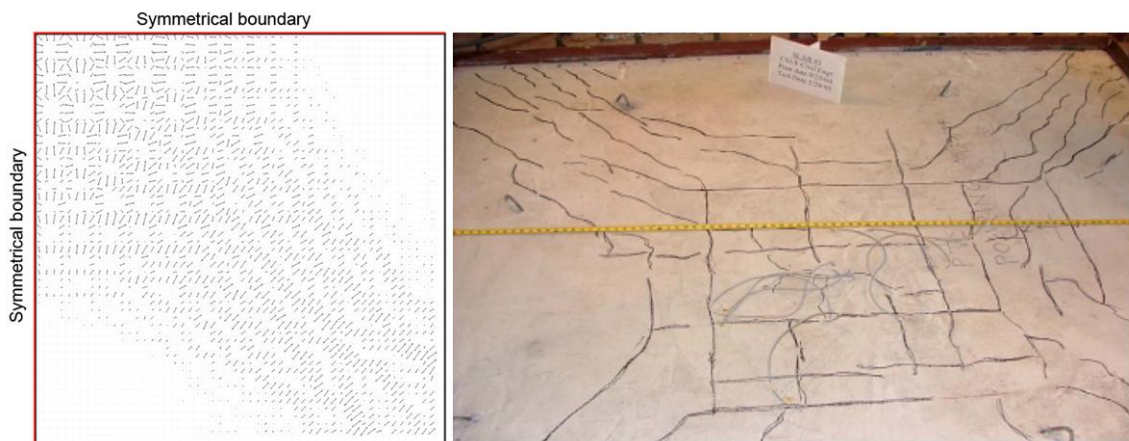


Fig. 8 Crack patterns (PTS-1)

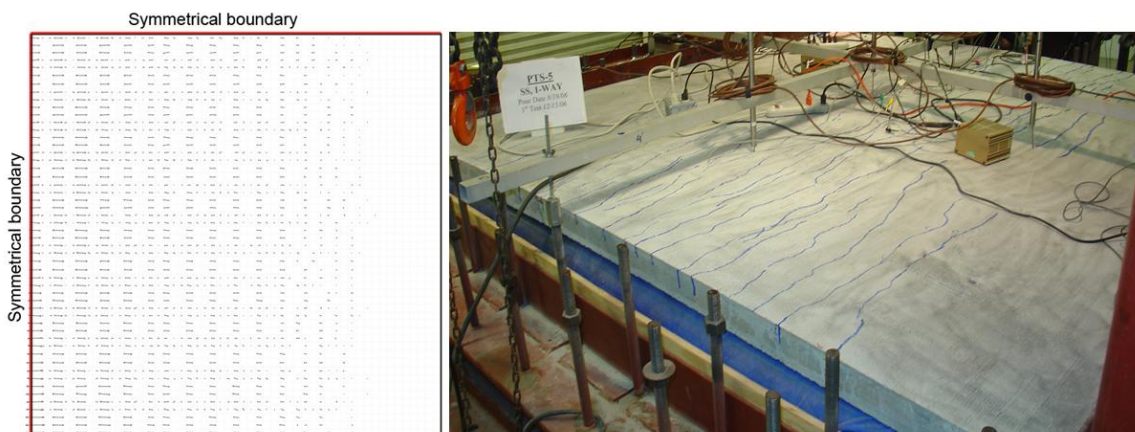


Fig. 9 Crack patterns (PTS-5)

moment was the largest (Fig. 9). Such crack patterns exhibited during the test are very similar to those obtained from numerical analyses. After the test, the bottom surfaces of the slabs were examined. Almost no cracking was observed on the bottom surface of the two-way slabs (i.e., no concrete crushing was noted). The testing was stopped when one of failure criteria was met. It is noted that special safety precautions are essential in the testing of an unbonded post-tensioning system.

4.2 Pressure (Uniformly distributed slab surface load) - deflection behavior

Figs. 10-12 show the pressure-deflection graphs of PTS-1, 3 & 5 to validate the accuracy of the proposed numerical model. In these comparison graphs, experimental test results are plotted in dotted lines and numerical simulation results are drawn in solid lines. In general, overall structural behaviors (pressure-deflection behavior) showed an excellent agreement between experimental &

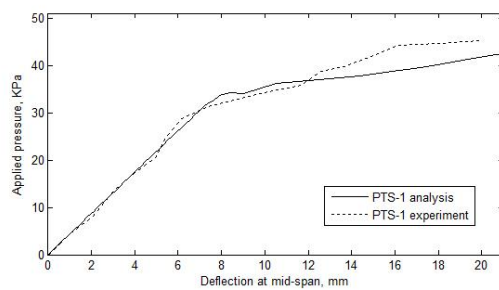


Fig. 10 Pressure-deflection relationship (PTS-1)

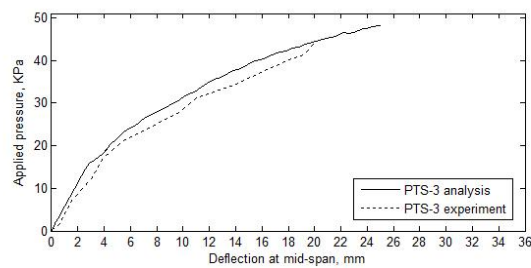


Fig. 11 Pressure-deflection relationship (PTS-3)

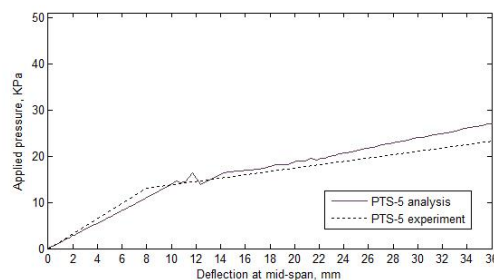


Fig. 12 Pressure-deflection relationship (PTS-5)

Table 3 Measured and simulated values at first cracking (P_{cr}) and maximum pressure (P_{max})

Specimen	Pressure at first cracking [P_{cr}], kPa (graph observation)			$P_{cr, Exp.} /$ $P_{cr, Num.}$	Maximum pressure [P_{max}], kPa		$P_{max, Exp.} /$ $P_{max, Num.}$
	Exp.		Num.		Exp.	Num.	
	Exp.	Num.	Exp.		Num.		
PTS-1	28.7	33.6	0.85	45.0	41.4	1.08	
PTS-3	17.0	19.5	0.87	45.0	44.1	1.02	
PTS-5	13.0	14.5	0.89	28.8	32.4	0.89	

Table 4 Measured and simulated pressure at the specific center deflections of the slabs

Specimen	Pressure at 3 mm deflection kPa			Pressure at 6 mm deflection kPa			Pressure at 10 mm deflection kPa			Pressure at 20 mm deflection kPa		
	Exp.	Num.	$\Delta Exp /$ ΔNum	Exp.	Num.	$\Delta Exp /$ ΔNum	Exp.	Num.	$\Delta Exp /$ ΔNum	Exp.	Num.	$\Delta Exp /$ ΔNum
	PTS-1	13.4	13.3	1.01	28.4	26.5	1.07	34	35	0.97	45	42
PTS-3	12.5	16.2	0.77	22.1	24.3	0.91	28	31	0.9	44	44	1
PTS-5*	4.9	4.1	1.20	8.3	9.9	0.84	14	14	1	17	19	0.89

*Excessive cracking

numerical results as shown in Figs. 10-12. Related to a two-way PT slab (PTS-1), the second slope of the bi-linear behavior starts around 34 kPa (with 8 mm deflection) for the numerical analysis model. Related to one-way PT slabs (PTS-3 and -5), these one-way slabs also showed an excellent agreement. So, overall behavior can be traced well through numerical simulation using developed PT slab models proposed in this study.

As observed in Figs. 10-12, the slabs behaved linearly during the initial stages of loading in general. The first crack (tension crack) appeared in any of the test slabs was defined as the hairline crack which occurred on the top of the slab and the corresponding pressure was defined as the pressure at the first cracking (Table 3). Once the two-way slab (PTS-1) cracked under about 28.7 kPa pressure, it exhibited reduced flexural stiffness as evidenced by the pressure-deflection relationships shown in Fig. 10. The second stage of the linear behavior of the cracked elastic slab continued until the yielding of non-prestressed mild steel began to occur under about 45.0 kPa pressure. As the flexural tensile cracks increased in number and width, the pressure-deflection curve started to show tri-linearity and slope reduction. After the mild steel yielding, a significantly reduced stiffness was noted. A similar tri-linear pressure-deflection behavior was also observed in the experiments of other two two-way slab specimens (PTS-2 and PTS-6).

Similar behavior of the one-way slab was noted. The boundary condition affected the pressure-deflection behavior. As the number of pinned supports changed from 0 to 1 to 2, the stiffness and load carrying capacity were reduced. Testing of PTS-5 with two pinned supports was stopped due to excessive cracking. The pressure-deflection relationship of the PTS-3 specimen with two fixed supports also became nonlinear rather than tri-linear (Fig. 11), while PTS-5 exhibited a distinctly

bi-linear pressure-deflection relationship (Fig. 12). This indicates that the initial stiffness and post-cracking behavior of unbonded PT slabs were improved by the increased fixity of the end supports. It is particularly important in terms of the serviceability of slender PT members. Hence, in order to minimize floor vibrations, application of restrained boundary conditions is strongly recommended. The stiffness degradation of one-way slabs was well reproduced by the developed nonlinear finite element model, which thus can be used to conduct a detailed vibration analysis of PT floors in the future.

Table 4 shows the comparison between measured and simulated pressure at the specific center deflections of the slabs. It can be noticed that nonlinear behavior of one-way and two-way slabs can be traced with accuracy through numerical simulations as shown in Table 4. To figure out the effect of boundary condition, the center deflection of PTS-3 (two fixed ends) is compared with those of PTS-5 (two pinned ends) in Table 4. It clearly shows that PTS-3 had a lot less center deflections compared to PTS-5 under the same pressure load.

4.3 Stresses in post-tensioning tendons and non-prestressed mild steel

Unlike bonded prestressed or conventionally reinforced concrete members, the prestressing strands in the unbonded post-tensioned members never reach their ultimate strength (f_{pu}). This is because the ultimate strength (f_{pu}) of unbonded tendons is not dependent on the localized strain at the flexural critical section, but depends on the total member elongation, number of spans and/or plastic hinges, span-to-depth ratio, and loading type (Kang and Wallace 2008, ACI Committee 318 2011). Just before loading of the slabs, the post-tensioning forces in the strands were recorded. The average effective stress (in this case before external loading) was normally kept between 65% and 70% of the ultimate strength of the strands. As the loading increased, the tendon stress increased nonlinearly. The rate of tendon stress increase was very small (about 0.005% of f_{se}) before concrete cracking, but became increasingly larger as the slab deflection increased until the ultimate load.

On the other hand, as the slabs were loaded and started to crack, the stress in the mild steel

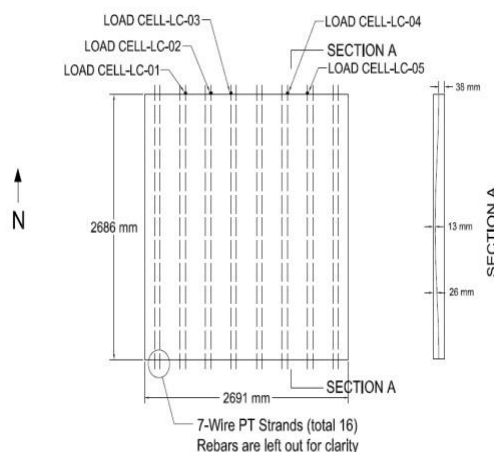


Fig. 13 Pinned-pinned one-way slab layout (PTS-5)

Table 5 Measured and simulated pressure at the specific center deflections of the slabs

Water pressure (kPa)	LC01 (kN)		LC02 (kN)		LC03 (kN)		LC04 (kN)		LC05 (kN)	
	Exp.	Num.								
0.0	31.3	28.4	29.9	28.4	30.0	28.4	30.6	28.4	30.6	28.4
3.4	31.3	28.5	29.9	28.5	30.0	28.6	30.6	28.5	30.6	28.5
6.9	31.4	28.7	29.9	28.7	30.0	28.7	30.6	28.7	30.6	28.7
10.3	31.5	28.8	29.9	28.8	30.0	28.9	30.6	28.8	30.6	28.8
13.1	31.5	28.9	29.9	29.0	30.0	29.0	30.6	28.9	30.7	28.9
13.8	31.5	29.0	29.9	29.0	30.0	29.0	30.5	29.0	30.7	29.0
17.2	32.2	29.7	30.6	29.8	30.6	29.9	31.0	29.8	31.3	29.7
20.7	32.8	30.5	31.4	30.6	31.3	30.7	31.7	30.6	32.0	30.5
24.1	33.5	31.1	32.1	31.2	31.9	31.4	32.3	31.2	32.7	31.1
27.6	34.1	31.8	32.8	31.9	32.5	32.0	33.2	31.9	33.3	31.8
28.8	34.3	32.0	32.9	32.1	32.7	32.3	33.3	32.1	33.4	32.0
Increase	0.66	0.81	0.68	0.84	0.61	0.87	0.61	0.83	0.62	0.81

started to increase and became close to yield stresses; however, no significant yielding was observed from the strain gauge data. For example, strain in the wire mesh of PTS-1 started to increase as the external loading was increased, and reached a maximum strain of about 0.002 at an external pressure on the slab of 45 kPa. The stresses of the wire mesh in the two-way slabs nearly reached the yield stress near the ultimate load, but it cannot be said that the nonlinear pressure-deflection behavior is attributed to the yielding of the mild steel. Rather, the nonlinear behavior was related to the significant concrete cracking. Note that the nonlinear behavior of the tendons was modest, as it was kept within the elastic range. Numerical analyses also verified that little mild steel yielding occurred.

Monitoring the unbonded PT forces through numerical simulation is very challenging due to the following reasons: a) contact and friction behavior between PT stands and sheathing; b) force transfer mechanism in the anchorage system; and c) actual tendon profile. In spite of these difficulties, according to Table 5 and Fig. 13, the increase pattern of PT strand forces can be traced using the proposed numerical model in this study. The measured increments in PT force are smaller than the numerical results. This is because the numerical model does not consider the friction losses along the PT tendons and the measured tendon forces were read from the load cells mounted at the end of tendons. However, the measured forces at 28.8 kPa water pressure were quite close to the numerical values, indicating that almost no friction appeared to exist between the concrete and the PT tendon at the ultimate stage and that the numerical model is quite reliable.

5. Conclusion

Based on the comparison between the experimental data and numerical analysis results, it is concluded that the numerical model developed as part of this study is capable of reproducing the behavior of post-tensioned one-way and two-way slabs with unbonded tendons, including the cracking occurrence and pattern, global pressure (uniformly distributed slab surface load) – deflection relationship, stiffness degradation due to cracking, influence of different boundary

conditions, stresses or forces in unbonded post-tensioning tendons and non-prestressed mild steel, and unbonded tendon stress distribution along the length of tendon at ultimate.

Acknowledgments

The work presented in this paper was funded by a NASA grant (FAR-NASA-2002) and a National Research Foundation of Korea grant (2012-005905). The authors also thank partial supports from Cal State Fullerton and from Seoul National University. The views expressed are those of authors, and do not necessarily represent those of the sponsors.

References

- ACI Committee 318 (2011), *Building code requirements for structural concrete (ACI 318-11) and commentary*, American Concrete Institute, Farmington Hills, MI, USA.
- Aroni, S. (1968), "Strength of slender prestressed concrete columns", *PCI J*, **13**(2), 19-33.
- ASTM (2008), *Annual book of ASTM standards*, American Society for Testing and Materials, West Conshohocken, PA, USA.
- Bondy, K.B. (2012), "Two-way post-tensioned slabs with bonded tendons", *PCI J*, **8**(2), 43-48.
- Carreira, D.J. and Chu, K.H. (1985), "Stress-strain relationship for plain concrete in compression", *ACI J Proceed*, **82**(6), 797-804.
- Chacos, G.P. (2007), "Back-up bars for residential slab-on-ground foundations", *PCI J*, **5**(1), 17-22.
- Devalapura, R.K. and Tadros, M.K. (1992), "Critical assessment of ACI 318 Eq. (18-3) for prestressing steel stress at ultimate flexure", *ACI Struct. J*, **89**(5), 538-546.
- Greunen, J.V. and Scordelis, A.C. (1983), "Nonlinear analysis of prestressed concrete slabs", *ASCE J Struct. Eng.*, **109**(7), 1742-1760.
- HKS (2011), *ABAQUS/CAE User's Manual*, Hibbit, Karlsson and Sorensen, Inc., Providence, RI, USA.
- Huang, Y., Kang, T.H.-K., Ramseyer, C. and Rha, C. (2010), "Background to multi-scale modelling of unbonded post-tensioned concrete structures", *Int. J. Theoretical and Applied Multiscale Mech.*, **1**(3), 219-235.
- Kang, T.H.-K. and Wallace, J.W. (2008), "Stresses in unbonded tendons of post-tensioned flat plate systems under dynamic excitation", *PTI J*, **6**(1), 31-44.
- Kim, U., Chakrabarti, P.R. and Choi, J. (2009), "Finite element analysis for inelastic flexural behavior of unbonded post-tensioned concrete beams", *5th International Structural Engineering & Construction Conference (Isec-5)*, Las Vegas, NV, September.
- Kim, U., Kang, T.H.-K., Huang, Y. and Chakrabarti, P.R. (2011), "Experimental and numerical analyses of unbonded PT one-way slabs with different boundary conditions", *The 2011 International Conference on Computational Technologies in Concrete Structures*, Seoul, Korea, September.
- Kim, U., Kang, T.H.-K. and Chakrabarti, P.R. (2012), "Rehabilitation of unbonded post-tensioned slabs with different boundary conditions", *PTI J*, **8**(2), 5-19.
- Klemencic, R., Fry, J.A., Hurtado, G. and Moehle, J.P. (2006), "Performance of post-tensioned slab-core wall connections", *PTI J*, **4**(2), 19-33.
- Kwak, H.G. and Son, J.K. (2010), "Inelastic behaviour of PSC beams with unbonded external tendons", *Mag. Concrete Res*, **62**(5), 313-326.
- PTI (2006), *Post-Tensioning Manual*, (6th Edition), Post-Tensioning Institute, Phoenix, AZ, USA.
- Rabczuk, T. and Zi, G. (2008), "Numerical fracture analysis of prestressed concrete beams", *Int J. Concrete Struct Mater*, **2**(2), 153-160.
- Scordelis, A.C., Lin, T.Y. and Itaya, R. (1959), "Behavior of continuous slab prestressed in two directions",

ACI J., **31**(6), 441-459.

Vecchio, F.J., Gauvreau, P. and Liu, K. (2006), "Modeling of unbonded post-tensioned concrete beams critical in shear", *ACI Mater. J.*, **103**(1), 57-64.

CC